Letter

Euler-obstructed nematic nodal superconductivity in twisted bilayer graphene

Jiabin Yu [1,*], Ming Xie [1], Fengcheng Wu [2,3] and Sankar Das Sarma [1]

[1] *Condensed Matter Theory Center and Joint Quantum Institute, Department of Physics, University of Maryland, College Park, Maryland 20742, USA*

[2] *School of Physics and Technology, Wuhan University, Wuhan 430072, China*

[3] *Wuhan Institute of Quantum Technology, Wuhan 430206, China*

(Received 21 February 2022; revised 13 April 2023; accepted 17 April 2023; published 9 May 2023)

Signatures of nematic nodal superconductivity have been experimentally observed in magic angle twisted bilayer graphene (MATBG). Here, we propose a general topological mechanism explaining how a nematic pairing leads to nodal superconductivity in MATBG. By focusing on the intervalley $C_{2z}\mathcal{T}$-invariant Cooper pairing order parameter, we show that the pairing order parameter can always be split into a trivial channel and an Euler obstructed channel, owing to the nontrivial normal-state band topology. When the pairing is spontaneously nematic, we find that a sufficiently-dominant Euler obstructed channel with two zeros typically leads to nodal superconductivity. The mechanism is general since it is independent of the specific interaction that accounts for the required pairing. Under the approximation of exactly-flat bands, we analytically find that the mean-field zero-temperature superfluid weight is bounded from below, and thus the Berezinksii-Kosterlitz-Thouless (BKT) critical temperature can be nonzero, even if the Euler obstructed pairing is dominant. We also numerically find that a spontaneously-nematic dominant Euler obstructed pairing can arise from a local attractive interaction.

DOI: 10.1103/PhysRevB.107.L201106

Introduction. The normal state of MATBG, (i.e., twisted bilayer graphene with twist angle near 1.1° [1–3]) was theoretically shown to host topologically nontrivial nearly-flat bands near the charge neutrality, based on the Bistritzer-MacDonald (BM) model [3–7]. The nontrivial band topology is characterized by the $C_{2z}\mathcal{T}$-protected nonzero Euler numbers [7] (or equivalently Wilson loop winding numbers [5]), where C_{nj} is the spinless part of the n-fold rotation about the j axis (with $j = z$ out of plane) and $\mathcal{T}$ is the spinful time-reversal symmetry. (Here the spinful $\mathcal{T}$ is effectively the same as the spinless time-reversal symmetry for the band topology, owing to the absence of spin-orbit coupling.) When the nearly-flat bands are partially filled, superconductivity was observed in MATBG [2,8–16], attracting huge theoretical interests [17–39]. In particular, experimental signatures of nematic nodal superconductivity were recently reported [12,14,15], when there are $2\sim 3$ holes per moiré unit cell. Here, being nematic means breaking C_{3z}.

In this letter, we propose a general mechanism explaining how a nematic pairing leads to nodal superconductivity in MATBG, based on the normal-state Euler numbers. Our mechanism clarifies the role of normal-state Euler numbers in the nematic nodal superconductivity of MATBG, which was missed by all previous works.

To be more specific, we consider the intervalley $C_{2z}\mathcal{T}$-invariant mean-field pairing order parameter that is either spin-singlet or spin-triplet with a momentum-independent spin direction, since the existing experiments suggest that $C_{2z}\mathcal{T}$ is crucial for the superconductivity in MATBG [14]. We find that the pairing order parameter can always be split into a trivial channel and a nontrivial channel. The nonzero normal-state Euler numbers require the pairing gap function of nontrivial channel to have zeros, and determine the total winding number of the zeros, whereas the trivial channel is allowed to have a nonvanishing pairing gap function. Thus, the nontrivial channel is called Euler obstructed. When the considered $C_{2z}\mathcal{T}$-invariant pairing is spontaneously nematic, we find that a sufficiently-dominant Euler obstructed channel with two zeros typically leads to nodal superconductivity, serving as a mechanism that connects the nematic pairing to nodal superconductivity. Our mechanism is general since it is independent of the specific interaction that accounts for the required pairing form.

We further analytically obtain a lower bound of the zero-temperature superfluid weight for the considered $C_{2z}\mathcal{T}$-invariant pairing under the exact-flat-band approximation, without assuming any specific interaction that accounts for the pairing. In particular, the lower bound of the superfluid weight holds even for pairings with a dominant Euler obstructed channel, meaning that their Berezinksii-Kosterlitz-Thouless (BKT) critical temperatures can be nonzero. Our result is beyond the previous-derived bound for the uniform s-wave pairing [40–44], since the uniform s-wave pairing does not contain the Euler obstructed channel. Numerically, we verify the above statements for the pairings given by a local attractive interaction; the interaction has a similar form as that mediated by acoustic phonons [23,25,26]. In particular, we find that a spontaneously-nematic pairing with a dominant Euler obstructed channel (that has two zeros) can arise from the local interaction. Therefore, our work suggests that nodal nature of the superconducting MATBG may arise from a dominant Euler obstructed pairing.

*jiabinyu@umd.edu

Euler obstructed Cooper pairing in MATBG. We start by introducing the Euler obstructed Cooper pairing in MATBG. The BM model contains two decoupled valley $\pm$ related by the C_{2z} or $\mathcal{T}$ symmetries, and within each valley, the model has $C_{2z}\mathcal{T}$, C_{3z}, and spin-charge U(2) symmetries. Because of the normal-state global spin SU(2) symmetry, we only need to consider the spinless parts for C_{nz}, as mentioned above. The model has other exact and approximate symmetries [5,45], but they are not required for the discussion below. With the twist angle θ near 1.1°, BM model captures the normal state of MATBG (that is not aligned with the hBN substrate [46]), and has two nearly-flat bands with additional spin degeneracy near the charge neutrality in each valley. We use $|u_{\pm,\boldsymbol{k},a}\rangle \otimes |s\rangle$ to label the periodic parts of the Bloch basis for the nearly-flat bands, where $a = 1, 2$ labels the spinless basis of the two nearly-flat bands in one valley, and $s =\uparrow, \downarrow$ is the spin index. Defining $|u_{\pm,\boldsymbol{k}}\rangle = (|u_{\pm,\boldsymbol{k},1}\rangle, |u_{\pm,\boldsymbol{k},2}\rangle)$, the nontrivial topology of $|u_{\pm,\boldsymbol{k}}\rangle$ is manifested by the nonzero Euler number or Wilson loop winding number $\mathcal{N}_\pm = 1$ [5,7,47].

For the superconductivity in MATBG, we only consider the pairing between the nearly-flat bands, owing to the large normal-state band gaps (∼20meV) above and below the nearly-flat bands. We consider the following mean-field Cooper pairing operator

$$H_{\text{pairing}} = \sum_{\boldsymbol{k}\in\text{MBZ}} c^\dagger_{+,\boldsymbol{k}} \Delta(\boldsymbol{k}) \otimes \Pi (c^\dagger_{-,-\boldsymbol{k}})^T + \text{H.c.}, \tag{1}$$

where $c^\dagger_{\pm,\boldsymbol{k}} = (\ldots, c^\dagger_{\pm,\boldsymbol{k},a,s}, \ldots)$ and $c^\dagger_{\pm,\boldsymbol{k},a,s}$ is the creation operator for the Bloch state of $|u_{\pm,\boldsymbol{k},a}\rangle \otimes |s\rangle$, and MBZ is short for moiré Brillouin zone. We have chosen and will always choose the pairing to be intervalley, since only the intervalley pairing can couple electrons with exactly the same energy and opposite momenta. Throughout the work, we also choose the pairing to be $C_{2z}\mathcal{T}$ invariant and to have a momentum-independent spin part Π. In particular, we consider two cases for Π, (i) spin-singlet $\Pi = is_y$ and (ii) spin-triplet $\Pi = i(\hat{n}\cdot \boldsymbol{s})is_y$ with $\hat{n}$ being any real momentum-independent unit vector, where $s_{x,y,z}$ are Pauli matrices for the spin index. For spin-triplet, we can always choose the spin index of the basis to keep $\hat{n} = (0, -1, 0)$, i.e., $\Pi = s_0$. The chosen pairing form is satisfied by certain solutions of the mean-field linearized gap equation owing to the $C_{2z}\mathcal{T}$ and spin SU(2) symmetries in the normal state [23,25,26], but remains an assumption at zero temperature. $\Delta(\boldsymbol{k})$ in Eq. (1) is the spinless part of the pairing gap function, which is the focus of our work.

Before our work, there were related discussions [28,46,48–52] on how the normal-state band topology affects $\Delta(\boldsymbol{k})$ in the Chern gauge [42,53–55] for $|u_{\pm,\boldsymbol{k}}\rangle$, which we specify below for our chosen pairing form. In the Chern gauge, $|u_{\pm,\boldsymbol{k},a}\rangle$ has well-defined Chern number $C_{\pm,a}$; we henceforth choose $C_{\pm,1} = -C_{\pm,2} = \mathcal{N}_\pm = 1$ and choose the following symmetry representations for the Chern gauge:

$$\begin{aligned}(C_{2z}\mathcal{T})c^\dagger_{\pm,\boldsymbol{k}}(C_{2z}\mathcal{T})^{-1} &= c^\dagger_{\pm,\boldsymbol{k}}\tau_x \otimes is_y\\ C_{2z}c^\dagger_{+,\boldsymbol{k}}C_{2z}^{-1} &= c^\dagger_{-,-\boldsymbol{k}},\end{aligned} \tag{2}$$

where τ's are the Pauli matrices for the spinless basis. Based on the Chern numbers of the paired Chern states [52], we can split $\Delta(\boldsymbol{k})$ into two channels as

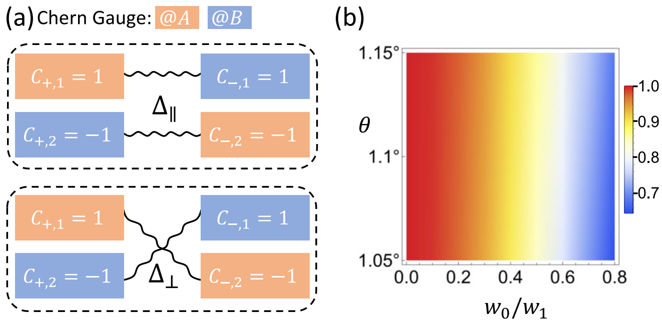

FIG. 1. (a) Schematic illustration of the two channels $\Delta_\parallel$ and $\Delta_\perp$ [Eq. (4)] in the Chern gauge. The blocks stand for the spinless basis for the nearly-flat bands in the Chern gauge, where $\pm$ stand for the valleys. The orange and purple blocks stand for the normal states that are polarized to the sublattice A and B [61], respectively, though the polarization may not be complete [49]. (b) Plot of the probability of $|u_{+,1}(\boldsymbol{k})\rangle$ in the Chern gauge at sublattice A averaged over the MBZ, showing the sublattice polarization discussed in Ref. [49,61]. w_0 and w_1 are the interlayer AB and AA tunneling strengths in the BM model, respectively.

$$\Delta(\boldsymbol{k}) = \Delta_\parallel(\boldsymbol{k}) + \Delta_\perp(\boldsymbol{k}), \tag{3}$$

where $\Delta_\parallel$ ($\Delta_\perp$) contains the pairings between Chern states with the same (opposite) Chern numbers [Fig. 1(a)] [56]. Owing to $C_2\mathcal{T}$ symmetry, we have

$$\Delta_\parallel(\boldsymbol{k}) = \begin{pmatrix} d^*_\parallel(\boldsymbol{k}) & \\ & d_\parallel(\boldsymbol{k})\end{pmatrix}, \quad \Delta_\perp(\boldsymbol{k}) = \begin{pmatrix} & d_\perp(\boldsymbol{k}) \\ d^*_\perp(\boldsymbol{k}) & \end{pmatrix}, \tag{4}$$

where $d_b(\boldsymbol{k}) = |\Delta_b(\boldsymbol{k})|e^{i\theta_b(\boldsymbol{k})}$ with $b = \perp, \parallel$, and $|\Delta_b(\boldsymbol{k})| = \sqrt{\text{Tr}[\Delta_b(\boldsymbol{k})\Delta_b^\dagger(\boldsymbol{k})]/2}$. If Δ_b has zeros (i.e., $|\Delta_b|$ has zeros) but is not everywhere-vanishing, an integer winding number can naturally be defined for each isolated zero i of Δ_b as

$$\mathcal{W}_{b,i} = -\frac{(-1)^b}{2\pi}\int_{\gamma_{b,i}} d\boldsymbol{k}\cdot\nabla_{\boldsymbol{k}}\theta_b(\boldsymbol{k}), \tag{5}$$

where $(-1)^\perp = 1$, $(-1)^\parallel = -1$, and $\gamma_{b,i}$ is a circle around the zero i of Δ_b. Then, Refs. [57,58] (which studied the pairing between Chern states) suggests that

$$\begin{aligned}\sum_i \mathcal{W}_{\perp,i} &= C_{+,1} + C_{-,2} = 0,\\ \sum_i \mathcal{W}_{\parallel,i} &= -C_{+,2} - C_{-,2} = 2.\end{aligned} \tag{6}$$

(See Supplemental Materials [59] for details.) As the total winding number $\sum_i \mathcal{W}_{b,i}$ is by definition zero if Δ_b has no zeros, Eq. (6) suggests that $\Delta_\parallel$ must have zeros, while $\Delta_\perp$ can be nonvanishing [52,57,58]. According to the terminology defined in Ref. [57], Eq. (4) and Eq. (6) suggest that each element of $\Delta_\parallel$ in the Chern gauge is a monopole Cooper pairing, since the nonzero total winding number indicates that the monopole harmonics [60] are required for the full description of $\Delta_\parallel$ in the Chern gauge. Thus, $\Delta_\parallel$ in the Chern gauge can be viewed as a $C_{2z}\mathcal{T}$-protected double version of monopole Cooper pairing.

The relation between $\Delta_\parallel$ and the monopole Cooper pairing relies on the Chern gauge, because the monopole Cooper pairing is only defined between Chern states. Nevertheless, as a generalization of the theory for 3D semimetals in Ref. [47], we find that the channel splitting into trivial $\Delta_\perp$ and nontrivial $\Delta_\parallel$ can be done for all gauges (even beyond the Chern gauge) by using the Wilson line and the gauge-invariant operator $P_\Delta(\boldsymbol{k}) = |u_{+,\boldsymbol{k}}\rangle \Delta(\boldsymbol{k}) \langle u^{C_{2z}\mathcal{T}}_{-,-\boldsymbol{k}}|$, where $|u^{C_{2z}\mathcal{T}}_{\pm,\boldsymbol{k}}\rangle = C_{2z}\mathcal{T}|u_{\pm,\boldsymbol{k}}\rangle$. The gauge transformations of the generally defined $\Delta_\parallel$ and $\Delta_\perp$ are the same as the guage transformation of Δ, meaning that $|\Delta_b(\boldsymbol{k})|$ and the zeros of $\Delta_b(\boldsymbol{k})$ are gauge invariant. Then, we can define the gauge-invariant winding number $W_{b,i}$ for the ith zero of $\Delta_b(\boldsymbol{k})$, and have

$$\sum_i \mathcal{W}_{b,i} = \mathcal{N}_+ - (-1)^b \mathcal{N}_- = 1 - (-1)^b. \tag{7}$$

(See Supplemental Materials [59] for details.) It means that the zeros of $\Delta_\parallel$ are generally enforced by the Euler numbers $\mathcal{N}_\pm$ for any gauges of the normal-state basis, even when the normal-state gauges do not have well-defined Chern numbers. In other words, Eq. (6) in Chern gauge is just a special case of the gauge-independent Eq. (7). Therefore, $\Delta_\parallel$ is called the Euler obstructed pairing channel. Our gauge-independent formalism is convenient for numerical calculations as it saves us from explicit gauge fixing.

Typically, the parity-even intersublattice pairing tends to have a dominant $\Delta_\parallel$, where the parity is equal (opposite) to the C_{2z} eigenvalue for the spin-singlet (spin-triplet) pairings. To show this, we can use the Chern gauge since $|\Delta_b|$ is gauge invariant. Based on Eq. (2) and Eq. (4), we find that $|\Delta_\parallel| = 0$ for parity-odd pairing, and thus only the parity-even pairing can have a dominant $\Delta_\parallel$. Then, since the states in the Chern gauge are polarized to the sublattice A or B of the BM model [49,61] [see also Fig. 1(b)], the parity-even $\Delta_\parallel$ ($\Delta_\perp$) mainly corresponds to intersublattice (intrasublattice) pairing.

Nematic nodal superconductivity in MATBG. Next we consider the case where the Euler obstructed pairing channel is sufficiently dominant, implying that $|\Delta_\perp|$ is perturbatively small compared to $|\Delta_\parallel|$ and the pairing is parity-even, and discuss the resultant nodal superconductivity. We only need to study the gapless nodes of the spin-up block of the Bogoliubov-de Gennes (BdG) Hamiltonian in + valley, whose matrix representation is labeled as $\mathcal{H}(\boldsymbol{k})$ for basis $(c^\dagger_{+,\boldsymbol{k},\uparrow}, c^T_{-,-\boldsymbol{k},\downarrow})$ with $c^\dagger_{\pm,\boldsymbol{k},s} = (c^\dagger_{\pm,\boldsymbol{k},1,s}, c^\dagger_{\pm,\boldsymbol{k},2,s})$; it is because the BdG gapless nodes are the same for the spin-down block owing to the normal-state spin SU(2) symmetry and the pairing form Eq. (1), and the BdG gapless nodes for the − valley can be obtained from the particle-hole symmetry. As the presence or absence of BdG nodes is gauge-independent, we use the Chern gauge for convenience, resulting in

$$\mathcal{H}(\boldsymbol{k}) = \begin{pmatrix} h_+(\boldsymbol{k}) - \mu & \Delta_\perp(\boldsymbol{k}) + \Delta_\parallel(\boldsymbol{k}) \\ [\Delta_\perp(\boldsymbol{k}) + \Delta_\parallel(\boldsymbol{k})]^\dagger & -h_+^T(\boldsymbol{k}) + \mu \end{pmatrix}, \tag{8}$$

where μ is the chemical potential, $h_+(\boldsymbol{k}) = \epsilon(\boldsymbol{k}) + \mathrm{Re}[f(\boldsymbol{k})]\tau_x + \mathrm{Im}[f(\boldsymbol{k})]\tau_y$ describes the normal-state nearly-flat bands in valley +, the form of $\Delta_b(\boldsymbol{k})$ is in Eq. (4), and we choose the zero-point energy such that $\epsilon(K_M) = 0$.

Owing to the parity-even nature of the pairing, $\mathcal{H}$ has an effective spinless $C_{2z}\mathcal{T}$ symmetry as $\rho_0\tau_x\mathcal{K}$ and a chiral symmetry $i\rho_y\tau_x$, belonging to the nodal class CI which can support stable zero-energy BdG gapless points protected by nonzero chiralities [62]. Here, $\mathcal{K}$ is the complex conjugate, and ρ's are the Pauli matrices for the particle-hole index. (See Supplemental Materials [59] for details.) In the following, we will discuss the $\Delta_\parallel$-guaranteed nodal superconductivity based on $\mathcal{H}$ for both C_{3z}-invariant and spontaneously nematic pairings. We choose $\mu \in [\epsilon(\Gamma_M) - |f(\Gamma_M)|, \epsilon(\Gamma_M) + |f(\Gamma_M)|]$, which is typically true for $2 \sim 3$ holes per moiré unit cell since the bottom and top of the set of nearly-flat bands are typically at Γ_M for realistic parameter values. (See Supplemental Materials [59] for details.) We also choose the Euler obstructed $\Delta_\parallel$ [or equivalently $d_\parallel(\boldsymbol{k})$] to only have two zeros with winding 1, since more zeros typically require more complex pairing structure which tends to be physically unfavored.

A sufficiently dominant $\Delta_\parallel$ guarantees $\mathcal{H}$ to be gapless only if $\mathcal{H}^{(0)}$ (which is $\mathcal{H}$ with $|\Delta_\perp| = 0$) is gapless. By diagonalizing $\mathcal{H}^{(0)}$, we find that $\mathcal{H}^{(0)}$ is gapless if and only if $\mu \in E(\Sigma)$, where Σ and $E(\Sigma)$ are defined in the following. Let us consider the deformation

$$d_\parallel(\boldsymbol{k}) \pm \lambda i f(\boldsymbol{k}), \tag{9}$$

where λ is gradually increased from 0 to 1. Owing to the normal-state Euler numbers, Eq. (9) must have zeros for all $\lambda \in [0, 1]$, since the deformation cannot merge the initial two zeros of $d_\parallel(\boldsymbol{k})$ that have the same winding. Then, the zeros of Eq. (9) for all $\lambda \in [0, 1]$ constitute Σ, and $E(\Sigma)$ consists of the values of $\epsilon(\boldsymbol{k}) \pm \sqrt{|f(\boldsymbol{k})|^2 - |d_\parallel(\boldsymbol{k})|^2}$ for all $\boldsymbol{k}$ in Σ. (See Supplemental Materials [59] for details.)

The difference between C_{3z}-invariant and spontaneously nematic pairings lies in the different shapes of Σ. $f(\boldsymbol{k})$ typically has two zeros at K_M and K'_M [Fig. 2(a)]. For C_{3z}-invariant pairing, the two zeros of $d_\parallel(\boldsymbol{k})$ are also pinned at K_M and K'_M by the C_{3z} symmetry. Then, Eq. (9) is typically zero at K_M and K'_M, meaning that the initial two zeros of $d_\parallel(\boldsymbol{k})$ typically does not move during the deformation. As a result, Σ is typically localized in the neighborhood of K_M and K'_M [the simplest case shown in Fig. 2(b)], and $E(\Sigma)$ only contains energies close to zero, leading to gapped $\mathcal{H}^{(0)}$ for considerably large μ. Therefore, a sufficiently-dominant $\Delta_\parallel$ cannot always guarantee nodal superconductivity when the pairing is C_{3z} invariant, even if fine-tuning cases are ruled out. We note that the specific value of μ needed for a gapped $\mathcal{H}^{(0)}$ varies with the form of $d_\parallel(\boldsymbol{k})$. For example, if $d_\parallel(\boldsymbol{k})$ has the same form as $f(\boldsymbol{k})$ and $f(\boldsymbol{k})$ takes the realistic form with only two zeros at K_M and K'_M, the nodal superconductivity can be gapped once μ is nonzero. (See Supplemental Materials [59] for details.)

On the other hand, for spontaneously nematic pairing, only one of the two zeros of $d_\parallel(\boldsymbol{k})$ is constrained by the C_{3z} eigenvalues, and is pinned at Γ_M. Then, without invoking fine tuning, there must be continuous paths connecting Γ_M to zeros of $d_\parallel(\boldsymbol{k}) \pm i f(\boldsymbol{k})$ [Fig. 2(c)], resulting that $\mu \in [\epsilon(\Gamma_M) - |f(\Gamma_M)|, \epsilon(\Gamma_M) + |f(\Gamma_M)|] \subset E(\Sigma)$ and then $\mathcal{H}^{(0)}$ has gapless nodes with nonzero chiralities. Therefore, when the pairing is spontaneously nematic, a sufficiently-dominant $\Delta_\parallel$ can always guarantee nodal superconductivity unless invoking fine tuning. (See Supplemental Materials [59] for details.)

The above mechanism for nematic nodal superconductivity is different from that discussed in Ref. [26] since the

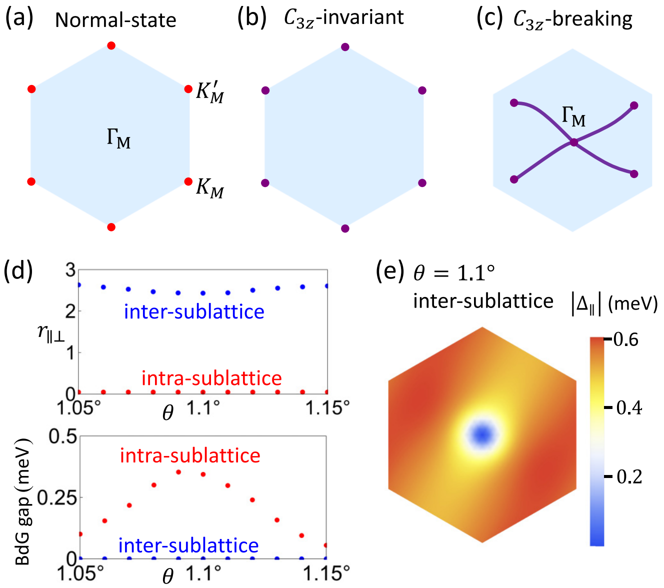

FIG. 2. (a) The normal-state Dirac cones [red dots, zeros of $f(\boldsymbol{k})$ in Eq. (8)] are typically located at K_M and K_M' in the MBZ (light blue). (b) Smallest Σ [defined below Eq. (9), purple] for C_{3z}-invariant pairing. (c) Illustrative Σ (purple) for spontaneously nematic pairing, when pinning both zeros of $\Delta_\parallel(\boldsymbol{k})$ at Γ_M. (d) Plots of the ratio $r_{\parallel\perp} = \langle|\Delta_\parallel|\rangle/\max(|\Delta_\perp|)$ and the BdG gap for the intrasublattice and intersublattice pairings induced by the local attractive interaction at zero temperature. θ is the twist angle, and $\langle|\Delta_b|\rangle$ and $\max(|\Delta_b|)$ are the averaged and maximum values of $|\Delta_b(\boldsymbol{k})|$ in the MBZ, respectively. (e) Plot of $|\Delta_\parallel|$ of the intersublattice pairing in the MBZ for $\theta = 1.1^\circ$ at zero temperature. $\Delta_\parallel(\boldsymbol{k})$ has two winding-1 zeros (or equivalently a winding-2 zero) at Γ_M, agreeing with the analogous discussion on the inter-Chern modes in Ref. [52].

latter does not involve any normal-state band topology. More importantly, the mechanism in Ref. [26] relies on a scalar pairing, which is not required in our work. (See Supplemental Materials [59] for details.)

The statements in the above discussion are independent of the specific form of the interaction that accounts for the pairing form Eq. (1). Nevertheless, we use a local attractive interaction, which has a similar form as that mediated by the acoustic phonons [23,25,26], to verify these general statements. According to Ref. [25], by tuning the interaction strength, we can get two types of $C_{2z}\mathcal{T}$-invariant intervalley parity-even pairings: C_{3z}-invariant intra-sublattice pairings and spontaneously-nematic inter-sublattice pairings. We obtain spin-triplet pairings of both types for 2.5 holes per moiré unit cell and $w_0/w_1 = 0.8$ by numerically solving the self-consistent equation, and find both the resultant intrasublattice and intersublattice pairings have the form in Eq. (1). By using the gauge-invariant formalism, we find that the intrasublattice and intersublattice pairings have dominant $\Delta_\perp$ and $\Delta_\parallel$ channels [Fig. 2(d)], respectively, agreeing with the above argument. Moreover, since the intersublattice pairing has two winding-1 zeros for $\Delta_\parallel$ [as exemplified in Fig. 2(e)], the corresponding BdG Hamiltonian must be nodal, which is also verified in Fig. 2(d). (See details in Supplemental Materials [59].) On the other hand, the C_{3z}-invariant intrasublattice pairing given by the local interaction has a dominant trivial pairing channel, which allows nodeless superconductivity [also consistent with Fig. 2(d)]. In short, the intersublattice pairing that we get from the local interaction is a spontaneously-nematic pairing that has an Euler obstructed channel dominant enough to guarantee nodal superconductivity.

Nodal superconductivity for the intervalley intersublattice pairing was also shown in Ref. [63]. The 2D nodal superconductivity in Ref. [63] is enforced by the normal-state chiral-symmetry-protected winding numbers, but the normal-state chiral symmetry is not exact in the BM model with realistic parameter values. In contrast, our mechanism relies on the normal-state $C_{2z}\mathcal{T}$-protected Euler numbers, which are exactly well-defined in the BM model with realistic parameter values.

Bounded superfluid weight. We now discuss lower bound of superfluid weight within the mean-field approximation. We adopt the exact-flat-band approximation [40–44], where we choose the normal-state flat bands to be exactly flat. By using the formalism of Euler obstructed Cooper pairing, we obtain a lower bound for the trace of the zero-temperature superfluid weight for the $C_{2z}\mathcal{T}$-invariant pairing in Eq. (1), which reads

$$\mathrm{Tr}[D_{SF}] \geqslant \left\langle \frac{[|\Delta_\perp(\boldsymbol{k})| - |\Delta_\parallel(\boldsymbol{k})|]^2}{\sqrt{[|\Delta_\perp(\boldsymbol{k})| - |\Delta_\parallel(\boldsymbol{k})|]^2 + \mu^2}} \right\rangle_g \frac{4e^2}{\pi}\mathcal{N}_+, \quad (10)$$

where we have chosen the unit system in which $\hbar = c = 1$, e is the elementary charge,

$$\langle x(\boldsymbol{k})\rangle_g = \frac{\int_{\mathrm{MBZ}} d^2k\, x(\boldsymbol{k})\, \mathrm{Tr}[g(\boldsymbol{k})]}{\int_{\mathrm{MBZ}} d^2k\, \mathrm{Tr}[g(\boldsymbol{k})]}, \quad (11)$$

and $g_{ij}(\boldsymbol{k}) = \frac{1}{2}\,\mathrm{Tr}[\partial_{k_i}P_+(\boldsymbol{k})\partial_{k_j}P_+(\boldsymbol{k})]$ is the Fubini-Study metric for $P_+(\boldsymbol{k}) = |u_{+,\boldsymbol{k}}\rangle\langle u_{+,\boldsymbol{k}}|$. If we choose the time-reversal-invariant uniform s-wave pairing used in Ref. [42], Eq. (10) reproduces the lower bound presented in Ref. [42]; however our Eq. (10) holds for any pairing of the form Eq. (1), even if the pairing is not uniform s-wave (like the intersublattice pairing in Fig. 2). For MATBG with θ very close to 1.1° and with pairings derived from the local attractive interaction mentioned above, the superfluid weight calculated from the exact-flat-band approximation is close to that directly calculated from the BM model with realistic band structure, meaning that the flat-band approximation is good for the study of the superfluid weight in this case. In this case, $\mathrm{Tr}[D_{SF}]$ estimated from the bound in Eq. (10) is roughly 10^8 H^{-1} for both intrasublattice and intersublattice pairings, similar to the values theoretically estimated in Ref. [42] and reported in Ref. [16], meaning that Eq. (10) is reasonably tight as a lower bound. (See details in Supplemental Materials [59].)

Discussion. In summary, we showed that a dominant Euler obstructed pairing channel serves as a general mechanism that connects a spontaneously-nematic pairing to nodal superconductivity in MATBG. The potential existence of a dominant Euler obstructed pairing in superconducting MATBG is supported by the bounded superfluid weight and the self-consistent numerical results.

Although topologically-obstructed order parameters have been studied in various works [46–48,57,58,64–69], those works are mainly focused on 3D systems, based on the topology of the bands on the Fermi surface (not the topology of the shape of the Fermi surface). Before our work, no 2D candidate superconductors were proposed for any topologically-obstructed Cooper pairing. Our work shows that MATBG is the first 2D realistic superconductor that potentially hosts a dominant topologically-obstructed Cooper pairing.

In this work, we allow several symmetries (like C_{2x}) of the BM model to be broken either spontaneously or externally in the normal state. An interesting direction is to study the interplay between these symmetries and the Euler obstructed Cooper pairing. Further systematic study of the underlying superconductivity may provide a reliable prediction on whether the Euler-obstructed Cooper pairing dominates in MATBG. As a speculation, the Euler-obstructed Cooper pairing might come from the competition between Coulomb and electron-phonon interaction that gives special interaction channels.

Acknowledgments. J.Y. thanks B. Andrei Bernevig, Yang-Zhi Chou, Zhi-Da Song, and in particular Jie Wang for helpful discussions. This work is supported by the Laboratory for Physical Sciences. F.W. is supported by startup funds of Wuhan University.

[1] Y. Cao, V. Fatemi, A. Demir, S. Fang, S. L. Tomarken, J. Y. Luo, J. D. Sanchez-Yamagishi, K. Watanabe, T. Taniguchi, E. Kaxiras *et al.*, Correlated insulator behaviour at half-filling in magic-angle graphene superlattices, Nature (London) **556**, 80 (2018).

[2] Y. Cao, V. Fatemi, S. Fang, K. Watanabe, T. Taniguchi, E. Kaxiras, and P. Jarillo-Herrero, Unconventional superconductivity in magic-angle graphene superlattices, Nature (London) **556**, 43 (2018).

[3] R. Bistritzer and A. H. MacDonald, Moiré bands in twisted double-layer graphene, Proc. Natl. Acad. Sci. USA **108**, 12233 (2011).

[4] H. C. Po, L. Zou, A. Vishwanath, and T. Senthil, Origin of Mott Insulating Behavior and Superconductivity in Twisted Bilayer Graphene, Phys. Rev. X **8**, 031089 (2018).

[5] Z. Song, Z. Wang, W. Shi, G. Li, C. Fang, and B. A. Bernevig, All Magic Angles in Twisted Bilayer Graphene are Topological, Phys. Rev. Lett. **123**, 036401 (2019).

[6] H. C. Po, L. Zou, T. Senthil, and A. Vishwanath, Faithful tight-binding models and fragile topology of magic-angle bilayer graphene, Phys. Rev. B **99**, 195455 (2019).

[7] J. Ahn, S. Park, and B.-J. Yang, Failure of Nielsen-Ninomiya Theorem and Fragile Topology in Two-Dimensional Systems with Space-Time Inversion Symmetry: Application to Twisted Bilayer Graphene at Magic Angle, Phys. Rev. X **9**, 021013 (2019).

[8] M. Yankowitz, S. Chen, H. Polshyn, Y. Zhang, K. Watanabe, T. Taniguchi, D. Graf, A. F. Young, and C. R. Dean, Tuning superconductivity in twisted bilayer graphene, Science **363**, 1059 (2019).

[9] X. Lu, P. Stepanov, W. Yang, M. Xie, M. A. Aamir, I. Das, C. Urgell, K. Watanabe, T. Taniguchi, G. Zhang, A. Bachtold, A. H. MacDonald, and D. K. Efetov, Superconductors, orbital magnets and correlated states in magic-angle bilayer graphene, Nature (London) **574**, 653 (2019).

[10] P. Stepanov, I. Das, X. Lu, A. Fahimniya, K. Watanabe, T. Taniguchi, F. H. L. Koppens, J. Lischner, L. Levitov, and D. K. Efetov, Untying the insulating and superconducting orders in magic-angle graphene, Nature (London) **583**, 375 (2020).

[11] Y. Saito, J. Ge, K. Watanabe, T. Taniguchi, and A. F. Young, Independent superconductors and correlated insulators in twisted bilayer graphene, Nat. Phys. **16**, 926 (2020).

[12] Y. Cao, D. Rodan-Legrain, J. M. Park, N. F. Q. Yuan, K. Watanabe, T. Taniguchi, R. M. Fernandes, L. Fu, and P. Jarillo-Herrero, Nematicity and competing orders in superconducting magic-angle graphene, Science **372**, 264 (2021).

[13] F. K. de Vries, E. Portolés, G. Zheng, T. Taniguchi, K. Watanabe, T. Ihn, K. Ensslin, and P. Rickhaus, Gate-defined josephson junctions in magic-angle twisted bilayer graphene, Nat. Nanotechnol. **16**, 760 (2021).

[14] M. Oh, K. P. Nuckolls, D. Wong, R. L. Lee, X. Liu, K. Watanabe, T. Taniguchi, and A. Yazdani, Evidence for unconventional superconductivity in twisted bilayer graphene, Nature (London) **600**, 240 (2021).

[15] G. D. Battista, P. Seifert, K. Watanabe, T. Taniguchi, K. C. Fong, A. Principi, and D. K. Efetov, Revealing the thermal properties of superconducting magic-angle twisted bilayer graphene, Nano Lett. **22**, 6465 (2022).

[16] H. Tian, S. Che, T. Xu, P. Cheung, K. Watanabe, T. Taniguchi, M. Randeria, F. Zhang, C. N. Lau, and M. W. Bockrath, Evidence for flat band dirac superconductor originating from quantum geometry, arXiv:2112.13401 [cond-mat.supr-con].

[17] C. Xu and L. Balents, Topological Superconductivity in Twisted Multilayer Graphene, Phys. Rev. Lett. **121**, 087001 (2018).

[18] H. Guo, X. Zhu, S. Feng, and R. T. Scalettar, Pairing symmetry of interacting fermions on a twisted bilayer graphene superlattice, Phys. Rev. B **97**, 235453 (2018).

[19] C.-C. Liu, L.-D. Zhang, W.-Q. Chen, and F. Yang, Chiral Spin Density Wave and $d + id$ Superconductivity in the Magic-Angle-Twisted Bilayer Graphene, Phys. Rev. Lett. **121**, 217001 (2018).

[20] H. Isobe, N. F. Q. Yuan, and L. Fu, Unconventional Superconductivity and Density Waves in Twisted Bilayer Graphene, Phys. Rev. X **8**, 041041 (2018).

[21] D. M. Kennes, J. Lischner, and C. Karrasch, Strong correlations and $d + id$ superconductivity in twisted bilayer graphene, Phys. Rev. B **98**, 241407(R) (2018).

[22] Y.-Z. You and A. Vishwanath, Superconductivity from valley fluctuations and approximate SO(4) symmetry in a weak coupling theory of twisted bilayer graphene, npj Quantum Mater. **4**, 16 (2019).

[23] F. Wu, A. H. MacDonald, and I. Martin, Theory of Phonon-Mediated Superconductivity in Twisted Bilayer Graphene, Phys. Rev. Lett. **121**, 257001 (2018).

[24] B. Lian, Z. Wang, and B. A. Bernevig, Twisted Bilayer Graphene: A Phonon-Driven Superconductor, Phys. Rev. Lett. **122**, 257002 (2019).

[25] F. Wu, E. Hwang, and S. Das Sarma, Phonon-induced giant linear-in-t resistivity in magic angle twisted bilayer graphene: Ordinary strangeness and exotic superconductivity, Phys. Rev. B **99**, 165112 (2019).

[26] F. Wu, Topological chiral superconductivity with spontaneous

vortices and supercurrent in twisted bilayer graphene, Phys. Rev. B **99**, 195114 (2019).
[27] D. V. Chichinadze, L. Classen, and A. V. Chubukov, Nematic superconductivity in twisted bilayer graphene, Phys. Rev. B **101**, 224513 (2020).
[28] E. Khalaf, S. Chatterjee, N. Bultinck, M. P. Zaletel, and A. Vishwanath, Charged skyrmions and topological origin of superconductivity in magic-angle graphene, Sci. Adv. **7**, eabf5299 (2021).
[29] Y. Wang, J. Kang, and R. M. Fernandes, Topological and nematic superconductivity mediated by ferro-su(4) fluctuations in twisted bilayer graphene, Phys. Rev. B **103**, 024506 (2021).
[30] M. Christos, S. Sachdev, and M. S. Scheurer, Superconductivity, correlated insulators, and wess–zumino–witten terms in twisted bilayer graphene, Proc. Natl. Acad. Sci. USA **117**, 29543 (2020).
[31] L. Classen, A. V. Chubukov, C. Honerkamp, and M. M. Scherer, Competing orders at higher-order van hove points, Phys. Rev. B **102**, 125141 (2020).
[32] V. Kozii, M. P. Zaletel, and N. Bultinck, Superconductivity in a doped valley coherent insulator in magic angle graphene: Goldstone-mediated pairing and kohn-luttinger mechanism, Phys. Rev. B **106**, 235157 (2022).
[33] S. Chatterjee, M. Ippoliti, and M. P. Zaletel, Skyrmion superconductivity: Dmrg evidence for a topological route to superconductivity, Phys. Rev. B **106**, 035421 (2022).
[34] E. Khalaf, P. Ledwith, and A. Vishwanath, Symmetry constraints on superconductivity in twisted bilayer graphene: Fractional vortices, 4e condensates or non-unitary pairing, arXiv:2012.05915 [cond-mat.supr-con].
[35] T. Cea and F. Guinea, Coulomb interaction, phonons, and superconductivity in twisted bilayer graphene, Proc. Natl. Acad. Sci. USA **118**, e2107874118 (2021).
[36] T. Yu, D. M. Kennes, A. Rubio, and M. A. Sentef, Nematicity Arising from a Chiral Superconducting Ground State in Magic-Angle Twisted Bilayer Graphene under In-Plane Magnetic Fields, Phys. Rev. Lett. **127**, 127001 (2021).
[37] G. Shavit, E. Berg, A. Stern, and Y. Oreg, Theory of Correlated Insulators and Superconductivity in Twisted Bilayer Graphene, Phys. Rev. Lett. **127**, 247703 (2021).
[38] C. Huang, N. Wei, W. Qin, and A. MacDonald, Pseudospin Paramagnons and the Superconducting Dome in Magic Angle Twisted Bilayer Graphene, Phys. Rev. Lett. **129**, 187001 (2022).
[39] Y. H. Kwan, G. Wagner, N. Bultinck, S. H. Simon, and S. A. Parameswaran, Skyrmions in Twisted Bilayer Graphene: Stability, Pairing, and Crystallization, Phys. Rev. X **12**, 031020 (2022).
[40] S. Peotta and P. Törmä, Superfluidity in topologically nontrivial flat bands, Nat. Commun. **6**, 8944 (2015).
[41] L. Liang, T. I. Vanhala, S. Peotta, T. Siro, A. Harju, and P. Törmä, Band geometry, berry curvature, and superfluid weight, Phys. Rev. B **95**, 024515 (2017).
[42] F. Xie, Z. Song, B. Lian, and B. A. Bernevig, Topology-Bounded Superfluid Weight in Twisted Bilayer Graphene, Phys. Rev. Lett. **124**, 167002 (2020).
[43] J. Herzog-Arbeitman, V. Peri, F. Schindler, S. D. Huber, and B. A. Bernevig, Superfluid Weight Bounds from Symmetry and Quantum Geometry in Flat Bands, Phys. Rev. Lett. **128**, 087002 (2022).
[44] P. Törmä, S. Peotta, and B. A. Bernevig, Superfluidity and quantum geometry in twisted multilayer systems, Nat. Rev. Phys. **4**, 528 (2022).
[45] Z.-D. Song, B. Lian, N. Regnault, and B. A. Bernevig, Twisted bilayer graphene. II. stable symmetry anomaly, Phys. Rev. B **103**, 205412 (2021).
[46] N. Bultinck, S. Chatterjee, and M. P. Zaletel, Mechanism for Anomalous Hall Ferromagnetism in Twisted Bilayer Graphene, Phys. Rev. Lett. **124**, 166601 (2020).
[47] J. Yu, Y.-A. Chen, and S. D. Sarma, Euler obstructed cooper pairing: Nodal superconductivity and hinge majorana zero modes, Phys. Rev. B **105**, 104515 (2022).
[48] S. Chatterjee, N. Bultinck, and M. P. Zaletel, Symmetry breaking and skyrmionic transport in twisted bilayer graphene, Phys. Rev. B **101**, 165141 (2020).
[49] N. Bultinck, E. Khalaf, S. Liu, S. Chatterjee, A. Vishwanath, and M. P. Zaletel, Ground State and Hidden Symmetry of Magic-Angle Graphene at Even Integer Filling, Phys. Rev. X **10**, 031034 (2020).
[50] J. Kang and O. Vafek, Non-abelian dirac node braiding and near-degeneracy of correlated phases at odd integer filling in magic-angle twisted bilayer graphene, Phys. Rev. B **102**, 035161 (2020).
[51] T. Soejima, D. E. Parker, N. Bultinck, J. Hauschild, and M. P. Zaletel, Efficient simulation of moiré materials using the density matrix renormalization group, Phys. Rev. B **102**, 205111 (2020).
[52] E. Khalaf, N. Bultinck, A. Vishwanath, and M. P. Zaletel, Soft modes in magic angle twisted bilayer graphene, arXiv:2009.14827 [cond-mat.str-el].
[53] F. N. Ünal, A. Bouhon, and R.-J. Slager, Topological Euler Class as a Dynamical Observable in Optical Lattices, Phys. Rev. Lett. **125**, 053601 (2020).
[54] A. Bouhon, Q. Wu, R.-J. Slager, H. Weng, O. V. Yazyev, and T. Bzdušek, Non-abelian reciprocal braiding of Weyl points and its manifestation in zrte, Nat. Phys. **16**, 1137 (2020).
[55] F. Xie, A. Cowsik, Z.-D. Song, B. Lian, B. A. Bernevig, and N. Regnault, Twisted bilayer graphene. VI. An exact diagonalization study at nonzero integer filling, Phys. Rev. B **103**, 205416 (2021).
[56] Channel splitting based on a different band topology in a different symmetry class was studied in Ref. [69].
[57] Y. Li and F. D. M. Haldane, Topological Nodal Cooper Pairing in Doped Weyl Metals, Phys. Rev. Lett. **120**, 067003 (2018).
[58] S. Murakami and N. Nagaosa, Berry Phase in Magnetic Superconductors, Phys. Rev. Lett. **90**, 057002 (2003).
[59] See Supplemental Material at http://link.aps.org/supplemental/10.1103/PhysRevB.107.L201106 for details on the Euler obstructed Cooper pairing in MATBG, the nodal superconductivity, and the bounded superfluid weight, which includes Refs. [70–77].
[60] T. T. Wu and C. N. Yang, Dirac monopole without strings: Monopole harmonics, Nucl. Phys. B **107**, 365 (1976).
[61] G. Tarnopolsky, A. J. Kruchkov, and A. Vishwanath, Origin of Magic Angles in Twisted Bilayer Graphene, Phys. Rev. Lett. **122**, 106405 (2019).
[62] T. c. v. Bzdušek and M. Sigrist, Robust doubly charged nodal lines and nodal surfaces in centrosymmetric systems, Phys. Rev. B **96**, 155105 (2017).

[63] C. F. B. Lo, H. C. Po, and A. H. Nevidomskyy, Inherited topological superconductivity in two-dimensional dirac semimetals, Phys. Rev. B **105**, 104501 (2022).

[64] C. Sun, S.-P. Lee, and Y. Li, Vortices in a monopole superconducting weyl semi-metal, arXiv:1909.04179.

[65] Y. Li, Berry phase enforced spinor pairing, arXiv:2001.05984.

[66] E. Muñoz, R. Soto-Garrido, and V. Juričić, Monopole versus spherical harmonic superconductors: Topological repulsion, coexistence, and stability, Phys. Rev. B **102**, 195121 (2020).

[67] M. J. Park, Y. B. Kim, and S. Lee, Geometric superconductivity in 3D hofstadter butterfly, arXiv:2007.16205.

[68] E. Bobrow, C. Sun, and Y. Li, Monopole charge density wave states in weyl semimetals, Phys. Rev. Res. **2**, 012078(R) (2020).

[69] C. Sun and Y. Li, z_2 topologically obstructed superconducting order, arXiv:2009.07263.

[70] P. A. Frigeri, D. F. Agterberg, A. Koga, and M. Sigrist, Superconductivity Without Inversion Symmetry: MnSi Versus $CePt_3Si$, Phys. Rev. Lett. **92**, 097001 (2004).

[71] C. Brouder, G. Panati, M. Calandra, C. Mourougane, and N. Marzari, Exponential Localization of Wannier Functions in Insulators, Phys. Rev. Lett. **98**, 046402 (2007).

[72] R. Yu, X. L. Qi, A. Bernevig, Z. Fang, and X. Dai, Equivalent expression of $\mathbb{Z}_2$ topological invariant for band insulators using the non-abelian berry connection, Phys. Rev. B **84**, 075119 (2011).

[73] Y.-Q. Ma, S.-J. Gu, S. Chen, H. Fan, and W.-M. Liu, The euler number of bloch states manifold and the quantum phases in gapped fermionic systems, EPL (Europhysics Letters) **103**, 10008 (2013).

[74] J. Ahn, D. Kim, Y. Kim, and B.-J. Yang, Band Topology and Linking Structure of Nodal Line Semimetals with Z_2 Monopole Charges, Phys. Rev. Lett. **121**, 106403 (2018).

[75] X. Hu, T. Hyart, D. I. Pikulin, and E. Rossi, Geometric and Conventional Contribution to the Superfluid Weight in Twisted Bilayer Graphene, Phys. Rev. Lett. **123**, 237002 (2019).

[76] A. Julku, T. J. Peltonen, L. Liang, T. T. Heikkilä, and P. Törmä, Superfluid weight and Berezinskii-Kosterlitz-Thouless transition temperature of twisted bilayer graphene, Phys. Rev. B **101**, 060505(R) (2020).

[77] L. Balents, C. R. Dean, D. K. Efetov, and A. F. Young, Superconductivity and strong correlations in moiré flat bands, Nat. Phys. **16**, 725 (2020).